

Stanisław Stupkiewicz

Finite element treatment of soft elastohydrodynamic lubrication problems in the finite deformation regime

Received: date / Accepted: date

Abstract Soft elastohydrodynamic lubrication problem is studied for a reciprocating elastomeric seal with full account of finite configuration changes. The fluid part is described by the Reynolds equation which is formulated on the deformed boundary of the seal treated as a hyperelastic body. The paper is concerned with the finite element treatment of this soft EHL problem. Displacement-based finite element discretization is applied for the solid part. The Reynolds equation is discretized using the finite element method or, alternatively, the discontinuous Galerkin method, both employing higher-order interpolation of pressure. The performance of both methods is assessed by studying convergence and stability of the solution for a benchmark problem of an O-ring seal. It is shown that the solution may exhibit spurious oscillations which occur in severe lubrication conditions. Mesh refinement results in reduction of these oscillations, while increasing the pressure interpolation order or application of the discontinuous Galerkin method does not help significantly.

Keywords Contact · Elastohydrodynamic lubrication · Finite element method · Discontinuous Galerkin method · Elastomeric seal

1 Introduction

Contact in the elastohydrodynamic lubrication (EHL) regime occurs when the two contacting surfaces are fully separated by the fluid and when the contact pressures are sufficiently high to cause significant elastic deflections of one or both contacting bodies. The EHL theory [6; 7] is a well developed theory with classical applications such as gears and rolling-contact bearings, which fall into the class of so-called hard EHL problems. There is, however, growing interest in the

soft EHL regime in which pressures are relatively low, but the elastic deflections are significant because one or both contacting bodies are soft. At the same time, the pressure is not high enough to cause significant increase of lubricant viscosity (on the contrary, the piezo-viscous effect is crucial in the hard EHL problems).

Soft EHL contact occurs, for instance, in the case of an elastomer in lubricated contact with a stiff surface; the typical examples are seals, windscreen wipers and wet tyres. However, soft EHL problems arise also in biotribological systems such as synovial joints, contact lens lubrication, eye-eyelid contact, human skin contact, and oral processing of food, see for instance Adams et al. [1], Dowson [5], Jones et al. [10], de Vicente et al. [29]. In the case of biotribological systems, additional difficulties are associated with constitutive modelling of soft tissues and biological fluids.

In this work, we specifically address the problem of hydrodynamic lubrication in reciprocating elastomeric seals. This is a classical topic studied experimentally and theoretically for more than 50 years, cf. Nau [17]. However, despite the substantial progress in computational techniques and increase of computer power, detailed solutions of the corresponding EHL problems are not easily found in the literature.

In the analysis of a typical EHL problem, two phenomena are considered, namely the flow of the lubricant in the thin film between the contacting bodies and the elastic deflections of the bodies. The fluid part is conveniently described using the Reynolds equation which relates the hydrodynamic pressure and the thickness of the lubricant film, see Section 3. At the same time, the film thickness results from the elastic deflections of the contacting bodies which are caused by the action of the hydrodynamic pressure. The two subproblems are thus strongly coupled.

In the EHL theory, the solid part is usually modelled within the linear elasticity framework. Furthermore, the elasticity problem is formulated for a half-space so that specialized solution methods can be applied, which employ analytical solutions available for point and line loads on an elastic half-space [6; 7]. Both assumptions (linear elasticity, half-space approximation) are fully adequate in the case of hard

S. Stupkiewicz
Institute of Fundamental Technological Research (IPPT)
Świętokrzyska 21, 00-049 Warsaw, Poland
Tel.: +48-22-8261281
Fax: +48-22-8269815
E-mail: sstupkie@ippt.gov.pl

EHL problems. However, this is not necessarily the case of soft EHL problems in which finite deformations may occur. Also the size of the contact zone may be comparable to the size of the contacting bodies so that half-space approximation is no longer justified.

For instance, in the case of elastomeric seals, the contact pressure may easily exceed the elastic shear modulus of the seal by one order of magnitude, hence finite deformations are expected, at least locally. Nevertheless, the early works on EHL in reciprocating seals relied on the linear elasticity assumption [24; 32]. The relation between the pressure and the elastic deflections was found using the finite element method, typically combined with static condensation. Similarly, a linear influence coefficient matrix can be determined also when a finite-deformation model is adopted for the elastomeric seal treated as a hyperelastic body. This matrix can be obtained from off-line finite element computations and subsequently used in the EHL solver, e.g., Prati and Strozzi [23], Salant et al. [25]. Nonlinear elasticity of an elastomeric seal has also been accounted for in a simplified model developed by Nikas and Sayles [19] for rectangular seals.

Recently, Stupkiewicz and Marciniszyn [28] derived a formulation of soft EHL problems in the finite deformation regime, with application for steady-state hydrodynamic lubrication in reciprocating elastomeric seals. The model takes full account of the finite configuration changes and coupling of the solid and fluid parts, including friction due to shear stresses in the lubricant film. Results of a detailed study of hydrodynamic lubrication and dynamic sealing performance are also provided for two benchmark problems, namely for O-ring and rectangular seals.

The present work addresses selected computational aspects of the formulation proposed by Stupkiewicz and Marciniszyn [28]. In addition to the finite element discretization, an alternative, discontinuous Galerkin treatment of the Reynolds equation is introduced following Lu et al. [14]. The performance of both methods is assessed by studying convergence and stability of the solution of the soft EHL problem for a reciprocating O-ring seal.

The paper is organized as follows. The formulation of the problem is provided in Sections 2 and 3 for the solid and fluid parts, respectively. This part is essentially a repetition of the corresponding part in [28]. Finite element treatment of the EHL problem at hand is discussed in Section 4, in which both the finite element method and the discontinuous Galerkin method are introduced for the Reynolds equation. Finally, the application for an elastomeric O-ring seal is presented in Section 5. Here, the main part (Section 5.2) is the study of the convergence of the solution with mesh refinement and other factors, such as pressure interpolation order.

2 Hyperelastic solid

The seal undergoes finite deformations caused by the action of the hydrostatic sealed pressure as well as by the contact

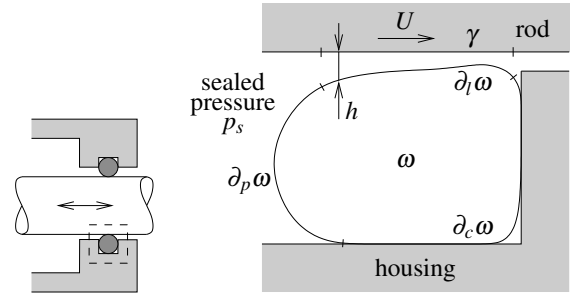


Fig. 1 Rod seal in the deformed configuration.

interactions with the housing and with the rod, the latter in the hydrodynamic lubrication regime. We assume that the housing and the rod are rigid. This simplifies the treatment of contact interactions. Note, however, that in some conditions the elastic deflections of the rod can be significant, e.g. for hollow-cylinder rods in high-pressure hydraulic systems, cf. Nikas [18].

Modelling of the solid part is rather standard. Two configurations are introduced—the stress-free initial configuration Ω and the deformed configuration ω . The boundary $\partial\Omega$ is divided into three non-overlapping parts $\partial_l\Omega$, $\partial_p\Omega$ and $\partial_c\Omega$ associated with the hydrodynamic lubrication, hydrostatic sealed pressure and contact interaction with the housing, respectively. The deformed-configuration counterparts are $\partial_l\omega$, $\partial_p\omega$ and $\partial_c\omega$, cf. Fig. 1. This division is not given *a priori* and, in general, depends on the deformation of the seal. This is commented more in Section 3.

The deformation from Ω to ω is given by a continuous mapping $\mathbf{x} = \boldsymbol{\varphi}(\mathbf{X})$, where $\mathbf{X} \in \Omega$ and $\mathbf{x} \in \omega$. In the absence of body and inertia forces, the weak form of the equilibrium equation reads

$$\int_{\Omega} \mathbf{P} \cdot \text{Grad } \delta \boldsymbol{\varphi} \, dV - \int_{\partial\Omega} \mathbf{T} \cdot \delta \boldsymbol{\varphi} \, dS = 0, \quad (1)$$

where \mathbf{P} is the first Piola–Kirchhoff stress tensor and \mathbf{T} is the nominal traction on the boundary $\partial\Omega$.

A hyperelastic material model is assumed for the elastomeric seal. The constitutive law is thus fully defined by the elastic strain energy function $W(\mathbf{F})$, namely

$$\mathbf{P} = \frac{\partial W}{\partial \mathbf{F}}, \quad (2)$$

where $\mathbf{F} = \partial \boldsymbol{\varphi} / \partial \mathbf{X} = \text{Grad } \boldsymbol{\varphi}$ is the deformation gradient. Specifically, a compressible Mooney–Rivlin material model is adopted with $W(\mathbf{F})$ given by

$$W(\mathbf{F}) = \frac{1}{2} \mu_1 (\bar{I}_1 - 3) + \frac{1}{2} \mu_2 (\bar{I}_2 - 3) + W_v(I_3), \quad (3)$$

where μ_1 and μ_2 are material parameters such that $\mu = \mu_1 + \mu_2$ is the shear modulus in the initial configuration. \bar{I}_1 , \bar{I}_2 and I_3 are the invariants of the left Cauchy–Green deformation tensor \mathbf{B} ,

$$\bar{I}_1 = \text{tr } \bar{\mathbf{B}}, \quad \bar{I}_2 = \frac{1}{2} (\bar{I}_1^2 - \text{tr } \bar{\mathbf{B}}^2), \quad I_3 = \det \mathbf{B}, \quad (4)$$

where

$$\mathbf{B} = \mathbf{F}\mathbf{F}^T, \quad \bar{\mathbf{B}} = I_3^{-1/3}\mathbf{B}. \quad (5)$$

The volumetric part $W_v(I_3)$ is given by

$$W_v(I_3) = \frac{1}{2} \kappa \left(\frac{1}{2}(I_3 - 1) - \frac{1}{2} \log I_3 \right), \quad (6)$$

where κ denotes the bulk modulus.

The Reynolds equation, as introduced in the next section, corresponds to the deformed configuration. Accordingly, the hydrodynamic pressure loading on $\partial_l \omega$, as well as the hydrostatic pressure loading on $\partial_p \omega$, are prescribed in the deformed configuration. The surface traction term in (1) is thus equivalently evaluated on the deformed boundary $\partial \omega$,

$$\int_{\partial \Omega} \mathbf{T} \cdot \delta \boldsymbol{\varphi} \, dS = \int_{\partial \omega} \mathbf{t} \cdot \delta \boldsymbol{\varphi} \, ds, \quad (7)$$

where \mathbf{t} is the *spatial* traction vector, i.e. one referred to the unit area in the deformed configuration.

The integrals in (7) are split into three parts corresponding to $\partial_p \omega$, $\partial_l \omega$ and $\partial_c \omega$. In the case of the hydrostatic pressure loading on $\partial_p \omega$, the surface traction is given by

$$\mathbf{t} = -p_s \mathbf{n} \quad \text{on } \partial_p \omega, \quad (8)$$

where p_s is the sealed pressure and \mathbf{n} is the unit outward normal in the deformed configuration. Specification of the traction on the lubricated contact boundary $\partial_l \omega$ is postponed to the next section.

Finally, the condition of frictionless contact along the contact boundary $\partial_c \omega$ is enforced using the Lagrange multiplier technique (e.g. Wriggers [30]), namely

$$\int_{\partial_c \omega} \mathbf{t} \cdot \delta \boldsymbol{\varphi} \, ds = \int_{\partial_c \omega} \lambda_N \delta g_N \, ds, \quad (9)$$

where the Lagrange multiplier λ_N and the normal gap g_N (defined such that $g_N > 0$ in case of separation) satisfy the Signorini condition,

$$g_N \geq 0, \quad \lambda_N \leq 0, \quad g_N \lambda_N = 0 \quad \text{on } \partial_c \omega. \quad (10)$$

In this work, the augmented Lagrangian technique is used to regularize the unilateral contact conditions (10). The details can be found in Alart and Curnier [2] and Pietrzak and Curnier [22].

3 Reynolds equation

The classical hydrodynamic lubrication theory is based on the well-known Reynolds equation, cf. Dowson and Higginson [6], Müller and Nau [16]. This equation describes the flow of a fluid (lubricant) in a thin channel between two solids in relative motion. It can be obtained by integrating the Navier-Stokes equation over the thickness of the fluid film under several assumptions of which the most important is the assumption that the film thickness is small compared to the other dimensions of the domain. It is further assumed that the pressure and viscosity are constant across the film

and that the flow is laminar so that a parabolic velocity profile is obtained. As a result the Reynolds equation expresses the mass conservation of the fluid in terms of the pressure and film thickness.

Importantly, the dimension of the problem is reduced so that the Reynolds equation is two-dimensional in the general case and one-dimensional if the flow does not depend on one spatial variable. Furthermore, the Reynolds equation is formulated in the Eulerian frame so that, in the case considered in this work, the Reynolds equation and all the quantities involved refer to the lubricated boundary $\partial_l \omega$ in the *deformed* configuration. As in the present model the rod is assumed to be rigid, it is convenient to introduce a domain, denoted by γ , which is a projection of the deformed boundary $\partial_l \omega$ onto the rigid surface of the rod, cf. Fig. 1. The Reynolds equation is then formulated on the domain γ .

For an incompressible fluid, the Reynolds equation takes the form

$$\operatorname{div}_\gamma \mathbf{q} + \frac{\partial h}{\partial t} = 0, \quad \mathbf{q} = \bar{\mathbf{u}} h - \frac{h^3}{12\eta} \operatorname{grad}_\gamma p, \quad (11)$$

where p is the hydrodynamic pressure, h the film thickness, \mathbf{q} the lubricant flux, $\bar{\mathbf{u}}$ the average velocity of the contacting surfaces, and η the viscosity. The gradient and divergence in Eq. (11) are defined on the surface γ , hence a subscript introduced in the respective operators. The essential and the natural boundary conditions are enforced on the respective parts of the boundary $\partial \gamma$, namely

$$p = p^* \quad \text{on } \partial_p \gamma, \quad \mathbf{q} \cdot \mathbf{n}_\gamma = q_n^* \quad \text{on } \partial_q \gamma, \quad (12)$$

where p^* is the prescribed pressure and q_n^* is the prescribed flux. Special boundary conditions have to be applied on the cavitation boundary—both the pressure and its gradient are prescribed at an unknown location which is found as a part of the solution, cf. [6]. This is avoided in this work by adopting a simple alternative approach (the penalty method [31]), as discussed in the next section.

At low pressures, typical for soft EHL problems, the dependence of viscosity on pressure (the piezo-viscous effect) is not much pronounced, however, for completeness, we introduce this dependence through the Barus equation,

$$\eta = \eta_0 \exp(\alpha p), \quad (13)$$

where α is the pressure-viscosity coefficient and η_0 is the viscosity at zero pressure. As isothermal conditions are only considered, the important temperature dependence of viscosity is not introduced.

Having in mind the numerical examples presented in Section 5, the Reynolds equation can be simplified significantly. Axial symmetry is assumed, so that the Reynolds equation becomes one-dimensional, and the term $\partial h / \partial t$ vanishes in steady-state conditions. The corresponding one-dimensional Reynolds equation reads

$$\frac{d}{d\bar{x}} \left(\bar{u} h - \frac{h^3}{12\eta} \frac{dp}{d\bar{x}} \right) = 0, \quad (14)$$

where $\bar{u} = U/2$, U is the rod speed (positive for outstroke, as indicated in Fig. 1, and negative for instroke), and the

spatial variable \bar{x} is a local variable which parameterizes γ . Equation (14) is accompanied by the boundary conditions

$$p(\bar{x}_s) = p_s, \quad p(\bar{x}_0) = 0, \quad (15)$$

which are enforced on the sealed-pressure side ($\bar{x} = \bar{x}_s$) and on the air side ($\bar{x} = \bar{x}_0$).

It is clear that the Reynolds equation in the form (14) states that the flux q given by the term in brackets is constant along the lubricated boundary. It is also seen that at the points of zero pressure gradient (e.g. at the point of maximum pressure) we have

$$q = \bar{u}h^*, \quad h^* = \frac{q}{\bar{u}} = \frac{2q}{U}, \quad (16)$$

where h^* is the characteristic thickness of the lubricant film. It further follows from Eq. (16) that the seal always leaks during outstroke (the flux q is positive for positive rod speed U). During instroke, the leaking fluid is (completely or partially) pumped back as the flux is then negative. The balance of the leakage during complete cycle determines whether the seal leaks—this is in brief the principle of the dynamic sealing mechanism, for more details see Müller and Nau [16].

The forces acting on the seal are due to the hydrodynamic pressure and shear stresses which develop in the lubricant film. The effect of shear stresses on the deformation of the contacting bodies is neglected in the classical EHL theory. In the present formulation it is fully accounted for and, as shown in Section 5, in some conditions the effect is not negligible.

The shear stress τ at the fluid-solid interface,

$$\tau = \frac{\eta U}{h} - \frac{h}{2} \frac{dp}{d\bar{x}}. \quad (17)$$

follows from the parabolic velocity profile across the film. Accordingly, the traction acting on the seal along the lubricated boundary $\partial_l \omega$ is given by

$$\mathbf{t} = -p\mathbf{n} + \tau\mathbf{s} \quad \text{on } \partial_l \omega, \quad (18)$$

where \mathbf{s} is the unit vector tangent to the nominal surface γ . Note that the hydrodynamic pressure loading is assumed in Eq. (18) to act along \mathbf{n} , the current normal to the *deformed* surface. Accordingly, \mathbf{n} and \mathbf{s} are not exactly perpendicular. However, thanks to this assumption, the hydrostatic and hydrodynamic pressure loading along, respectively, $\partial_p \omega$ and $\partial_l \omega$, are treated consistently. In practical terms, this gives quite some freedom in choosing the point of transition from the hydrostatic pressure loading to the hydrodynamic lubrication regime, provided this point is sufficiently far¹ from the actual contact zone.

Finally, we provide the weak form of the Reynolds equation which constitutes the basis of the finite element formulation. The weak form is obtained in a standard manner.

¹ Far from the actual contact zone the film thickness h is much higher than in this zone. In view of Eq. (11)₂, the pressure gradient quickly converges to zero when h increases. Accordingly, if the film thickness at the points at which the boundary conditions (15) are enforced is sufficiently high, then the results are practically insensitive to the positions of these points.

Equation (11)₁ is multiplied by the test function δp , vanishing on $\partial_p \gamma$, and integrated over the domain γ . Application of the Gauss theorem results in the following weak form

$$\int_{\gamma} \left(\text{grad}_{\gamma} \delta p \cdot \mathbf{q} - \delta p \frac{\partial h}{\partial t} \right) d\gamma - \int_{\partial_q \gamma} \delta p q_n^* dl = 0, \quad (19)$$

which corresponds to the general case specified by Eqs. (11) and (12).

4 Finite element treatment

The complete EHL problem is specified by the mechanical equilibrium equation (the solid part) and the Reynolds equation (lubrication), expressed by the variational weak forms (1) and (19), respectively. The virtual work of surface tractions, i.e. the second term in Eq. (1), is split into three parts corresponding to the hydrostatic pressure on $\partial_p \omega$, contact with the housing on $\partial_c \omega$, and hydrodynamic lubrication on $\partial_l \omega$.

The coupling of the two sub-problems is through the dependence of the film thickness h on the deformation (displacements) of the seal. At the same time, the loading acting on the seal along the boundary $\partial_l \omega$ is due to the hydrodynamic pressure p and shear stresses τ , cf. Eq. 18, which result from the solution of the Reynolds equation.

The finite element formulation is obtained by introducing the approximations of the unknown displacement and pressure fields, followed by element-wise numerical integration of the respective contributions (c.f. Zienkiewicz and Taylor [33]). As a result a set of nonlinear equations is obtained for unknown nodal quantities.

Finite element treatment of the solid part is standard, so the details are omitted here. A displacement-based formulation is derived from the weak form (1) and low-order elements are used which employ special techniques in order to avoid spurious locking effects. Specifically, two types of axisymmetric four-node elements are used, namely the F-bar element developed by de Souza Neto et al. [27] and an underintegrated element based on the volumetric-deviatoric split and Taylor expansion of shape functions (the latter element is a nonlinear version of the element developed by Korelc and Wriggers [13], see also Korelc [12]).

As regards the Reynolds equation, the finite element formulation is introduced below for the simplified steady-state case with the essential boundary conditions enforced on the whole boundary $\partial \gamma$, so that the weak form (19) simplifies to

$$\int_{\gamma} \text{grad}_{\gamma} \delta p \cdot \mathbf{q} d\gamma = 0. \quad (20)$$

The finite element equations are obtained by introducing a partition \mathcal{P}_{γ}^h of the domain γ into elements γ_{el} and a corresponding continuous finite element approximation of the pressure field, so that the integration in Eq. (20) can be performed element-wise,

$$\sum_{\gamma_{el} \in \mathcal{P}_{\gamma}^h} \int_{\gamma_{el}} \text{grad}_{\gamma} \delta p \cdot \mathbf{q} d\gamma = 0. \quad (21)$$

In addition to the classical continuous finite element discretization above, we apply also the discontinuous Galerkin method in which the approximating function is allowed to be discontinuous at the interfaces between elements. The corresponding formulation for the Reynolds equation has been introduced by Lu et al. [14], following the work of Baumann and Oden [4], and reads

$$\sum_{\gamma_{el} \in \mathcal{D}_\gamma^h} \int_{\gamma_{el}} \text{grad}_\gamma \delta p \cdot \mathbf{q} d\gamma - \int_{l_{\text{int}}} [p\mathbf{n}] \cdot \langle \delta \mathbf{q} \rangle dl + \int_{l_{\text{int}}} [\delta p \mathbf{n}] \cdot \langle \mathbf{q} \rangle dl = 0. \quad (22)$$

The second term and the third term in Eq. (22) weakly enforce the continuity of pressure and the flux balance, respectively. These terms are evaluated along interelement boundaries l_{int} on which the jump operator $[\cdot]$ and the average operator $\langle \cdot \rangle$ are defined as follows, cf. Zienkiewicz et al. [34],

$$[p\mathbf{n}] = p^- \mathbf{n}^- + p^+ \mathbf{n}^+, \quad \langle \mathbf{q} \rangle = \frac{1}{2}(\mathbf{q}^- + \mathbf{q}^+), \quad (23)$$

where \mathbf{n}^- and \mathbf{n}^+ are the outward normals at the element boundaries. Similar definitions hold for δp and $\delta \mathbf{q}$, the latter being defined by

$$\delta \mathbf{q} = -\frac{h^3}{12\eta} \text{grad}_\gamma \delta p. \quad (24)$$

As mentioned in the previous section, special treatment is necessary on the cavitation boundary. The cavitation condition implies that $p \geq p_{\text{cav}}$, where p_{cav} is the cavitation pressure assumed here equal to zero, $p_{\text{cav}} = 0$. Within the penalty method, cf. Wu [31], negative pressures are penalized by an extra term added to Eq. (21),

$$\sum_{\gamma_{el} \in \mathcal{D}_\gamma^h} \int_{\gamma_{el}} [\text{grad}_\gamma \delta p \cdot \mathbf{q} d\gamma + \varepsilon \delta p \max(-p, 0)] = 0, \quad (25)$$

where $\varepsilon > 0$ is the cavitation penalty parameter, and similarly in the discontinuous Galerkin formulation, cf. Lu et al. [15].

In the continuum formulation, the domain γ is a projection of the *deformed* boundary $\partial_l \omega$ on the rod surface. Consequently, the partition of γ into finite elements is introduced by the projection of the segments constituting the discretized boundary $\partial_l \omega$. In view of finite configuration changes, the domain γ and its partition into elements depend on the displacements of the seal (which are a part of the solution of the EHL problem at hand). This constitutes an additional coupling of the solid and lubrication parts.

The important consequence of using *low-order* solid elements is that the boundary, including the lubricated boundary $\partial_l \Omega$, is discretized into linear segments with piecewise-linear approximation of displacements. This implies linear interpolation of the film thickness h within each segment (first-order interpolation, $m_h = 1$) as the rod surface is rigid and, due to axial symmetry, represented by a line. However,

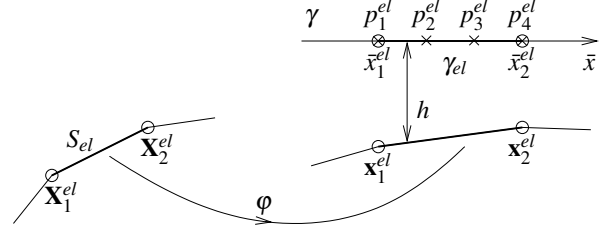


Fig. 2 Linear segment on the lubricated boundary $\partial_l \Omega$, here sketched for $m_p = 3$ so that there are $m_p + 1 = 4$ pressure nodes per element.

arbitrary interpolation order m_p can be adopted for the pressure p . Accordingly, the interpolation within a typical segment S_{el} is, cf. Fig. 2,

$$\mathbf{x} = \sum_{i=1}^2 N_i^{(1)} \mathbf{x}_i^{el} = \sum_{i=1}^2 N_i^{(1)} (\mathbf{X}_i^{el} + \mathbf{u}_i^{el}), \quad (26)$$

and

$$p = \sum_{i=1}^{m_p+1} N_i^{(m_p)} p_i^{el}, \quad (27)$$

where \mathbf{x}_i^{el} , \mathbf{X}_i^{el} , \mathbf{u}_i^{el} , and p_i^{el} are the nodal quantities, and $N_i^{(k)}$ are polynomial shape functions of order k . Clearly, in view of Eq. (26) we have

$$\bar{x} = \sum_{i=1}^2 N_i^{(1)} \bar{x}_i^{el}, \quad h = \sum_{i=1}^2 N_i^{(1)} h_i^{el}, \quad (28)$$

where the nodal quantities \bar{x}_i^{el} and h_i^{el} follow from straightforward considerations.

Importantly, increasing the pressure interpolation order results only in a small overhead on the total number of unknowns and on the overall computational cost. In the convergence studies presented in Section 5, interpolation orders ranging from $m_p = 1$ (linear interpolation) to $m_p = 5$ are used in the case of both the finite-element and the discontinuous-Galerkin treatment of the Reynolds equation.

The nonlinear equations resulting from the finite element discretization are solved monolithically for all global unknowns (displacements, pressures and Lagrange multipliers, the later enforcing the unilateral contact conditions) using the iterative Newton method. The exact tangent matrix, required in the Newton method, is obtained by linearization of the finite element equations. Here, all the dependencies related to the coupling of the solid and lubrication parts, mentioned earlier in this section, have to be taken into account. Naturally, the global tangent matrix is not symmetric.

In order to ensure convergence of the Newton method (the problem at hand is highly nonlinear due to finite configuration changes, elastohydrodynamic coupling, cavitation, etc.), a kind of path-following solution strategy has been developed. Firstly, for a given sealed pressure p_s , a frictionless contact problem is solved in which frictionless contact conditions (9) are enforced on $\partial_l \omega$ and solution of the Reynolds equation along $\partial_l \omega$ is suppressed. In the next step, the frictionless contact is gradually replaced by the lubricated contact by introducing a weighting factor which scales the respective nodal forces along $\partial_l \omega$. At this stage a relatively

Table 1 O-ring seal: geometrical, process and material parameters.

Inner diameter of the seal, D_{inner}	50.39	mm
Diameter of the seal, D_{seal}	3.53	mm
Rod diameter, D_{rod}	50.00	mm
Inner diameter of the housing, D_{housing}	56.30	mm
Rod speed, U	± 25 –1600	mm/s
Sealed pressure, p_s	0–5	MPa
Elastic parameter, μ_1	3.04	MPa
Elastic parameter, μ_2	0.62	MPa
Elastic bulk modulus, κ	500	MPa
Oil viscosity (HLP 46) at 30°C, η_0	$6.59 \cdot 10^{-8}$	MPa s
Pressure-viscosity coefficient, α	0.02	1/MPa
Cavitation penalty parameter, ε	10^4	mm/(MPa s)

high rod speed U is assumed, as this makes solution of the EHL problem easier. Finally, the rod speed is gradually decreased to the desired value. In fact, the last step directly provides the response for a range of rod speeds (at a fixed sealed pressure) which is a desired result of a typical analysis.

Computer implementation has been performed in the *AceGen/AceFEM* environment (Korelc [11; 12]). In this environment, the *AceGen* symbolic code generation system is used to automatically derive the characteristic expressions (such as the element residual vector and element tangent matrix) and to generate the corresponding optimized numerical code. The computations are then carried out in the *AceFEM* finite element environment.

5 Application for O-ring seal

The main goal of the study presented in this section is to illustrate the performance, accuracy and convergence behaviour of the proposed numerical scheme. An O-ring seal is chosen as a benchmark example and the corresponding EHL problem is defined in Section 5.1. Selected results illustrating hydrodynamic lubrication of the O-ring seal in reciprocating motion are also provided as an introduction to subsequent sections. Convergence of the results with the refinement of mesh and pressure interpolation order is studied in Section 5.2. Finally, the effect of pressure dependence of viscosity (piezo-viscous effect) is illustrated in Section 5.3.

5.1 Hydrodynamic lubrication in reciprocating O-ring seal

The analysis below is carried out for a reciprocating rod seal. Hydrodynamic lubrication in steady-state conditions is studied during both *outstroke* (the rod moves towards the air side, $U > 0$) and *instroke* (the rod moves towards the sealed-pressure side, $U < 0$). The general arrangement of the seal-rod-housing system is shown in Fig. 1, and the geometrical and process parameters are provided in Table 1. The elastic properties of the elastomeric seal (NBR rubber, 70 ShA hardness) and the viscosity of the hydraulic fluid (Shell Tellus 46 oil) at the working temperature of 30°C are also given in Table 1.

Table 2 O-ring seal: number of unknowns ($m_p = 4$).

	Total No. of unknowns	No. of pressure unknowns
mesh density 1	1076	109
mesh density 2	3587	217
mesh density 4	12929	433
mesh density 8	48893	865
mesh density 16	189941	1729

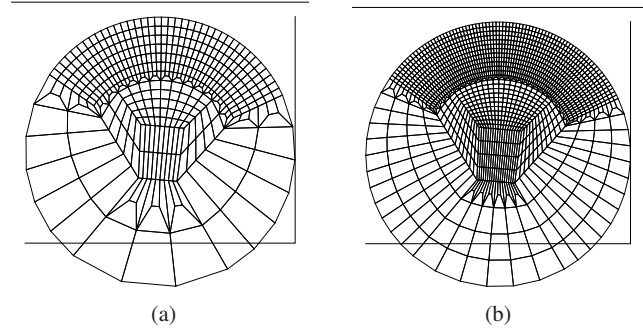


Fig. 3 O-ring seal in the initial undeformed configuration: finite element mesh for (a) mesh density 1 and (b) mesh density 2. The contact surfaces of the rod and housing are indicated by solid lines. The rod is on the top and the sealed-pressure side is on the left.

Five densities of the structured finite-element mesh have been used in the convergence studies presented in Section 5.2. Based on these studies, the finest mesh density 16 and pressure interpolation order $m_p = 4$ have been used in the computations reported below in order to ensure reliable results in the whole range of process parameters covered by the present study.

The total number of unknowns (displacements, pressures and contact Lagrange multipliers) is provided in Table 2 for the five mesh densities. The number of pressure unknowns in the Reynolds equation is also given in Table 2. These numbers correspond to the pressure interpolation order $m_p = 4$.

The mesh is significantly refined in the vicinity of the lubricated boundary. The undeformed mesh is shown in Fig. 3 for the mesh density 1 and 2. Subsequent finer meshes are obtained by repetitively decreasing the element size by the factor of two.

The deformation pattern is shown in Fig. 4. At the sealed pressure $p_s = 0$, the cross-section is compressed between the rod and the housing, and it is gradually pressed into the air-side corners as the sealed pressure increases, cf. Fig. 4(b–d). As a result, the contact zone expands at the air side and the shape of the free surface changes (e.g., the apparent radius decreases with increasing pressure). At the same time, the sealed-pressure side is not visibly affected by the variation of the pressure. Short vertical lines in Fig. 4 indicate the domain γ on which the Reynolds equation is solved.

The results that follow illustrate the influence of the process parameters on the solution of the EHL problem at hand. The profile of the hydrodynamic pressure p and the thickness h of the lubricant film at both outstroke and instroke are shown in Fig. 5 for two values of the sealed pressure p_s . The

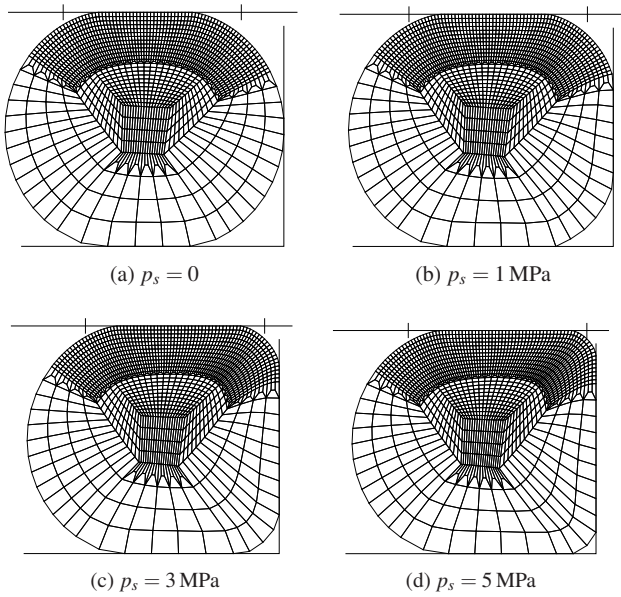


Fig. 4 O-ring seal in the deformed configuration: finite element mesh (mesh density 2) for different values of the sealed pressure p_s .

inlet and outlet zones are magnified in Fig. 6 (for $p_s = 2$ MPa only). Finally, Fig. 7 illustrates the effect of the rod speed U on the pressure and film thickness, and the corresponding details of the pressure profile are shown in Fig. 8. In all these figures, the position $\bar{x} = 0$ corresponds to the center of the cross-section in the initial configuration, as shown in Fig. 3.

It is seen that qualitative features of the solution depend only on the direction in which the rod moves, i.e. whether outstroke or instroke is considered. The main difference between the two cases is that, in the case of instroke, a sudden drop of pressure occurs next to the position of minimum film thickness at the sealed-pressure side. In the case of outstroke, an analogous pressure drop at the air side is excluded due to cavitation (in fact, it is obtained if the cavitation condition is not enforced).

The film thickness decreases towards the outlet zone with a sharp minimum at the end of the actual contact zone. In the inlet and outlet zones, the film thickness increases quickly. Note, however, that the lines, which seem almost vertical in Figs. 5(b) and 7(b), correspond to the inclination angle of 10–15 degrees (note the different scaling of the horizontal and vertical axes).

The actual thickness of the lubricant film is sensitive to all process parameters: it is smaller at instroke than at outstroke and it strongly decreases if the rod speed decreases. Furthermore, the film thickness decreases with increasing sealed pressure at instroke, while an opposite, but weaker effect is observed at outstroke. All these dependencies are illustrated in Fig. 9 in which parameter h^* is shown as a function of the sealed pressure p_s at selected values of the rod speed U . Recall that parameter h^* is the film thickness at the point of maximum pressure. This parameter is also a

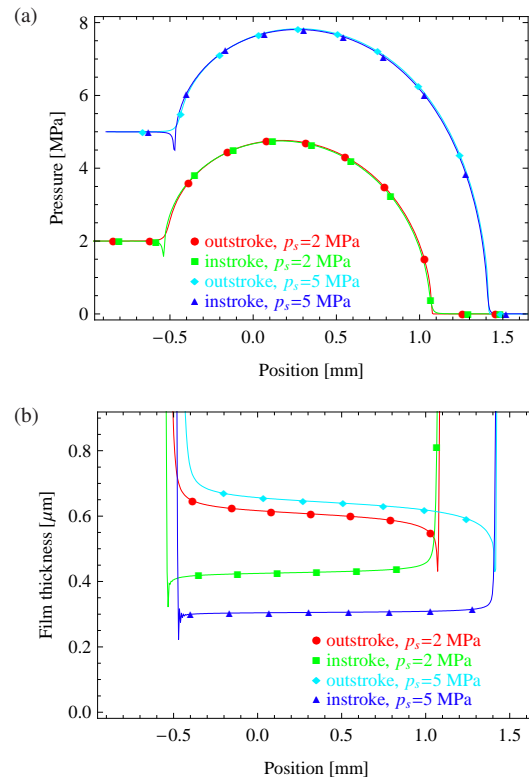


Fig. 5 Distribution of (a) pressure p and (b) film thickness h for two values of the sealed pressure p_s at the rod speed $U = 100$ mm/s.

convenient measure of the leakage rate in view of the relation (16).

The effect of the rod speed on the fine features of the pressure profile in the inlet and outlet zones is illustrated in Fig. 8. The general trend is that for lower rod speed the inlet and outlet zones are smaller and the pressure converges more quickly to the values prescribed as boundary conditions ($p = p_s$ or $p = 0$).

Except in the inlet and outlet zones, the pressure is mainly affected by the value of the sealed pressure p_s , cf. Figs. 5(a) and 7(a). As the film thickness is small compared to the dimensions of the cross-section, the pressure profile is, in fact, very close to that corresponding to a pure contact analysis. This is, by the way, the basic assumption of the simplified *inverse hydrodynamic theory*, cf. Müller and Nau [16].

Finally, let us note that relatively small changes of the pressure profile, visible mostly in the inlet and outlet zones, are associated with significant changes of the lubricant film thickness and of the related leakage rate. Accordingly, exact resolution of the inlet and outlet zones is crucial for accurate solution of the EHL problem at hand.

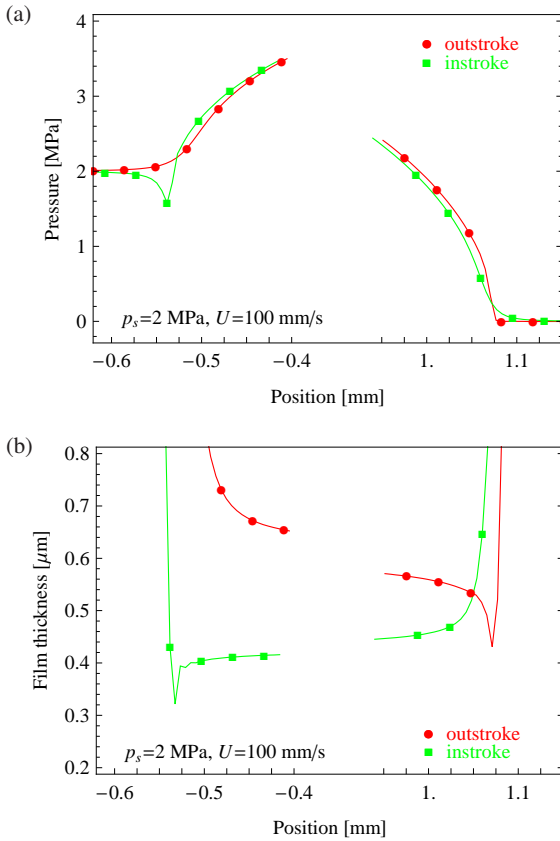


Fig. 6 Details of the inlet and outlet zones of the diagrams presented in Fig. 5: (a) pressure p and (b) film thickness h .

5.2 Convergence studies

In order to assess the performance of the numerical scheme presented in Section 4, convergence studies have been performed by applying different mesh densities and pressure interpolation orders for the solution of the O-ring example of the previous subsection.

Initial studies revealed that oscillations of pressure and film thickness occur in some situations. As a possible remedy for this problem, the discontinuous Galerkin method has been used in addition to the classical (continuous) finite element treatment of the Reynolds equation, following the promising results of Lu et al. [14; 15] obtained for the hard EHL problems. Accordingly, both the finite element (FE) and the discontinuous Galerkin (DG) method have been implemented and used in the present study. Note that oscillatory solutions have already been reported for heavily loaded hard EHL contacts solved with the use of the finite element method, e.g. [8; 20], and also for soft EHL problems in elastomeric seals [23].

The oscillations mentioned above are clearly visible in Fig. 10, which shows convergence of the solution with mesh refinement for the pressure interpolation order $m_p = 4$. It is seen that the mesh refinement reduces these oscillations. In the present case of outstroke at the sealed pressure $p_s =$

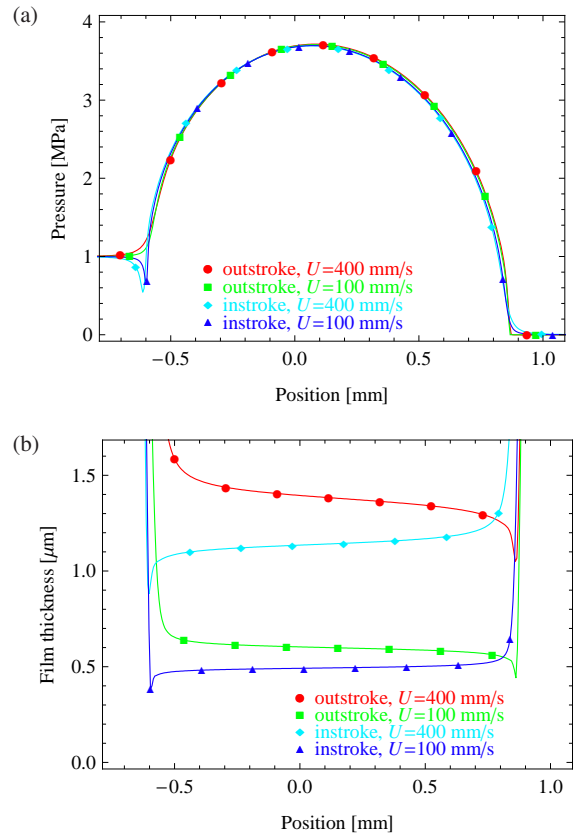


Fig. 7 Effect of rod speed U on (a) pressure p and (b) film thickness h at the sealed pressure $p_s = 1$ MPa.

1 MPa and rod speed $U = 400$ mm/s, an oscillation-free (and apparently converged) solution is obtained for mesh density 4 and higher. However, upon magnification it is seen that the resolution of the dip in film thickness is improved when the mesh is further refined up to mesh density 16, see Fig. 11. The results in Figs. 10 and 11 correspond to the FE treatment of the Reynolds equation, the results obtained using the DG method are very similar and are thus omitted here.

Figure 12 presents the pressure distributions obtained for mesh density 2 using different values of the pressure interpolation order m_p . In the case of both FE and DG method, the pressure converges quickly with increasing interpolation order so that the pressures corresponding to $m_p = 4$ and $m_p = 5$ are hardly distinguished in Fig. 12. As the results are obtained for a low mesh density 2, the converged pressure distributions exhibit oscillations.

In the case of the DG method, the discontinuities of pressure at the interelement boundaries are clearly visible for $m_p = 1$ and quickly decrease for higher interpolation orders, cf. Fig. 12(b). For instance, the maximum pressure jump is equal to 0.24 MPa for $m_p = 4$ and 0.10 MPa for $m_p = 5$. The discontinuities of pressure decrease with the refinement of mesh so that the corresponding jumps are 0.043 MPa and 0.015 MPa for mesh density 4, and are below 0.002 MPa for mesh density 8.

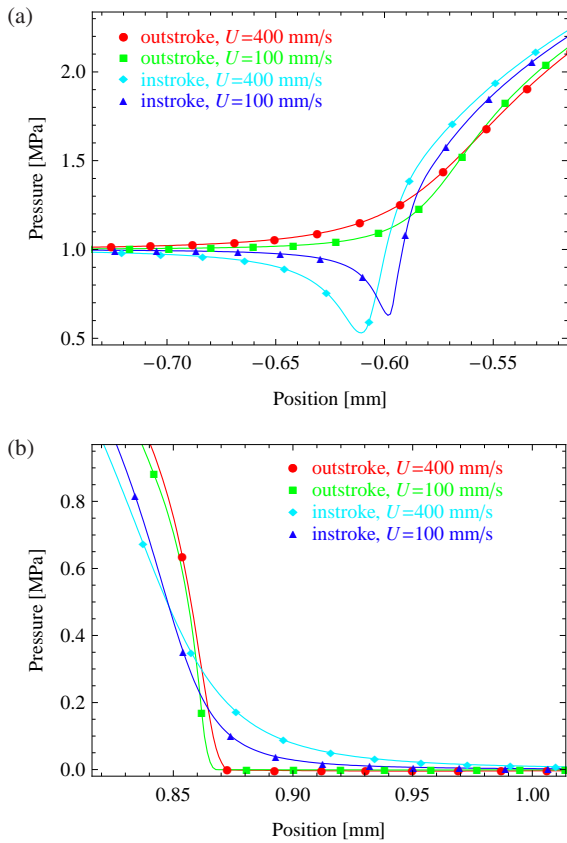


Fig. 8 Details of the pressure profile shown in Fig. 7(a): (a) sealed-pressure side, (b) air side.

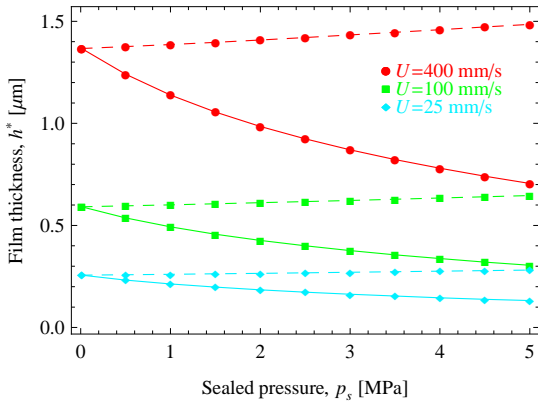


Fig. 9 Parameter $h^* = q/\bar{u}$ as a function of the sealed pressure p_s (instroke – solid lines, outstroke – dashed lines).

One of the important conclusions of the present analysis is that the DG method does not perform noticeably better than the continuous FE method as regards the spurious oscillations of pressure and film thickness. This is illustrated in Figs. 13 and 14 showing the effect of the rod speed U on the film thickness for the FE and DG treatment of the Reynolds equation. Solutions corresponding to rod speeds ranging from 25 to 800 mm/s are shown for both outstroke and instroke (note the logarithmic scale on the plots). It is

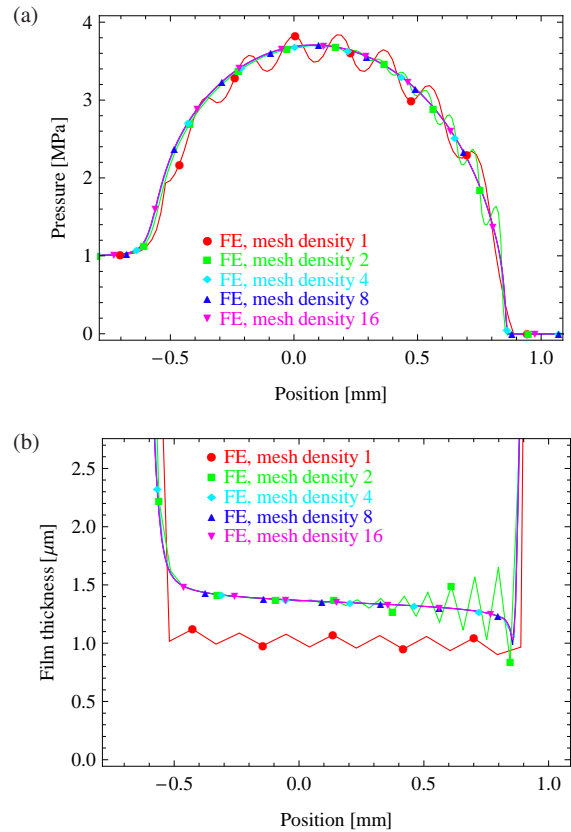


Fig. 10 Convergence with mesh refinement: (a) pressure p and (b) film thickness h for different mesh densities (FE treatment of the Reynolds equation, $m_p = 4$, outstroke, $p_s = 1$ MPa, $U = 400$ mm/s).

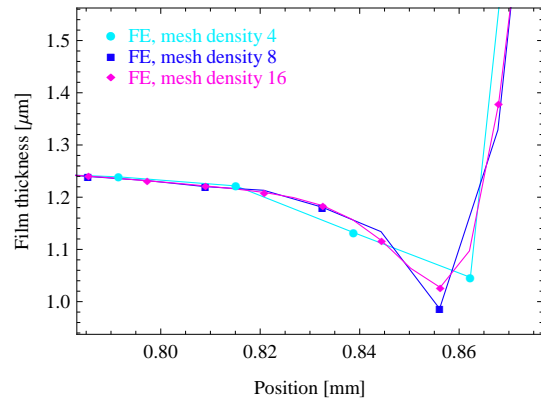


Fig. 11 Film thickness h for mesh densities 4, 8 and 16 – detail of the diagram in Fig. 10(b).

seen that the oscillations appear at $U = 200$ mm/s and are more pronounced for decreasing rod speed and film thickness. The results obtained using the FE and DG method do not differ significantly.

The effect of both the rod speed and the mesh density is shown in Fig. 15. We note that the higher the mesh density the lower the rod speed at which oscillations appear. In the present case (outstroke, $p_s = 5$ MPa), small oscillations are

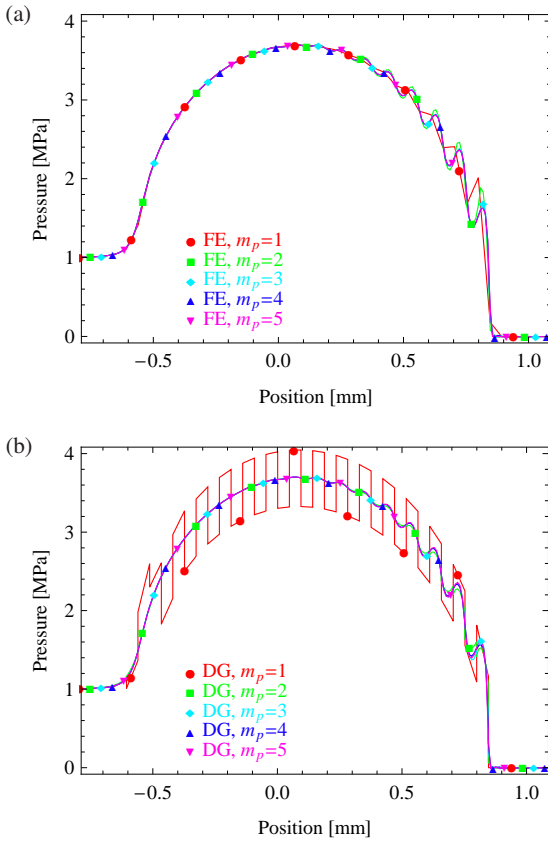


Fig. 12 Distribution of pressure p for (a) FE and (b) DG treatment of the Reynolds equation and for different pressure interpolation orders m_p (mesh density 2, outstroke, $p_s = 1$ MPa, $U = 400$ mm/s).

visible for $U = 50$ mm/s even for the finest mesh density 16, while for mesh density 8 the oscillations appear for $U = 200$ mm/s.

The general conclusion is that spurious oscillations of the solution may occur in severe lubrication conditions, and the severer the lubrication conditions the finer mesh is necessary to avoid these oscillations. Low rod speed leading to low film thickness is the main factor that promotes the oscillations. Severe conditions are also associated with higher sealed pressures and with the instroke (rather than outstroke).

Importantly, a solution with mild oscillations may still provide reasonable estimation of the actual profile of pressure and film thickness—note the similarity of the film thickness profiles corresponding to different mesh densities in Fig. 15 once the oscillations are filtered out.

The above observation is also confirmed by the quick convergence of the parameter $h^* = q/\bar{u}$ with the refinement of mesh, particularly for high pressure interpolation order, cf. Fig. 16. Consider, for instance, mesh density 2, for which an oscillatory solution is obtained, cf. Fig. 12. Nevertheless, in the case of the FE treatment of the Reynolds equation, parameter h^* predicted for $m_p = 2$ is only 1% lower than the converged value, and the error is below 0.3% for $m_p \geq 3$.

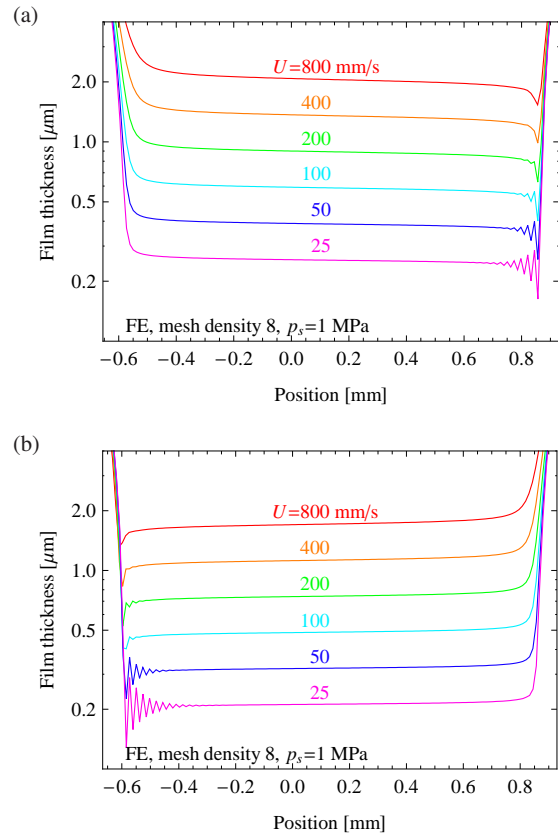


Fig. 13 FE treatment of the Reynolds equation: effect of the rod speed U on the film thickness h for (a) outstroke and (b) instroke (mesh density 8, $m_p = 4$).

From Fig. 16 it follows that, as regards the accuracy of the predictions of the leakage rate represented by parameter h^* , the performance of the DG method is somewhat worse than in the case of the FE treatment of the Reynolds equation. Note, however, that h^* has been determined differently in both cases. In the case of FE method, the lubricant flux q has been determined at the Gauss points and its value (taken at the middle of the contact zone) has been used to compute h^* from Eq. (16). In the case of DG method, the film thickness has been taken directly at the point of maximum pressure (both fields have been smoothed beforehand).

In the course of development and testing of the present numerical scheme, several attempts have been undertaken directed at avoiding or reducing the spurious oscillations. In particular, the influence of the formulation of solid elements used to model hyperelastic deformations of the seal has been checked. Two types of elements were available for the study, cf. Section 4, and their performance has been compared. No visible effect of the formulation on the oscillations has been observed while the convergence of parameter h^* with mesh refinement seems to be slightly worse in the case of F-bar element, cf. Fig. 17. Accordingly, the element based on volumetric-deviatoric split and Taylor expansion of shape

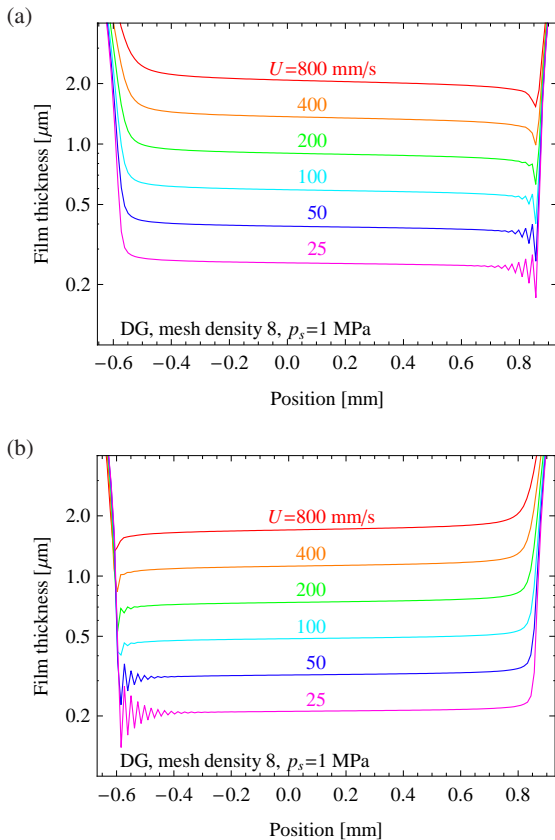


Fig. 14 DG treatment of the Reynolds equation: effect of the rod speed U on the film thickness h for (a) outstroke and (b) instroke (mesh density 8, $m_p = 4$).

functions has been used in all the computations reported in this work.

Finally, the effect of the quadrature used for numerical integration of the Reynolds equation has been investigated. It is well known that interface elements are prone to oscillatory solutions and that the oscillations are reduced if the Gauss quadrature is replaced, for instance, by the Lobatto quadrature, cf. Schellekens and de Borst [26]. It turns out that in the present case the oscillations are not affected by the choice of integration scheme. As the convergence with mesh refinement is concerned, the effect of the integration scheme is only visible for mesh densities 1 and 2 and for low pressure interpolation order, $m_p \leq 2$, both in the case of FE and DG method. Sample results are presented in Fig. 18.

5.3 Piezo-viscous effect

As already mentioned, the piezo-viscous effect, i.e. pressure dependence of viscosity, is by far less important in the case of soft EHL problems than in the case of hard EHL problems. For instance, considering hydraulic seals, the viscosity increases only 1.8 times at a relatively high pressure of 30 MPa (for a typical value of pressure-viscosity coefficient $\alpha = 0.02$ 1/MPa) and 1.2 times at the pressure of 8 MPa,

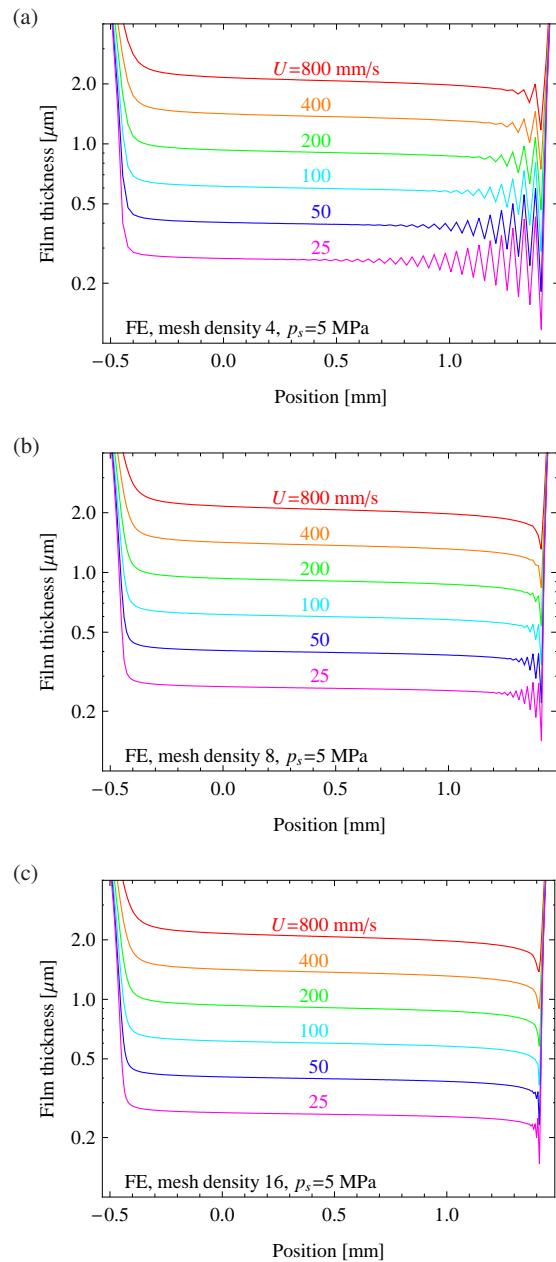


Fig. 15 Effect of the rod speed U and mesh density on the film thickness h : (a) mesh density 4, (b) mesh density 8, (c) mesh density 16 (FE treatment of the Reynolds equation, $m_p = 4$).

the maximum pressure encountered in the example studied above. However, the piezo-viscous effect can be easily included in the modelling by adopting the Barus equation (13), and thus it has been fully accounted for in the computations reported above.

For completeness, in this subsection we briefly illustrate the effect that pressure dependence of viscosity has on the hydrodynamic lubrication of the O-ring seal. Film thickness, corresponding to both constant viscosity $\eta = \eta_0$ and variable viscosity governed by the Barus equation (13), is shown

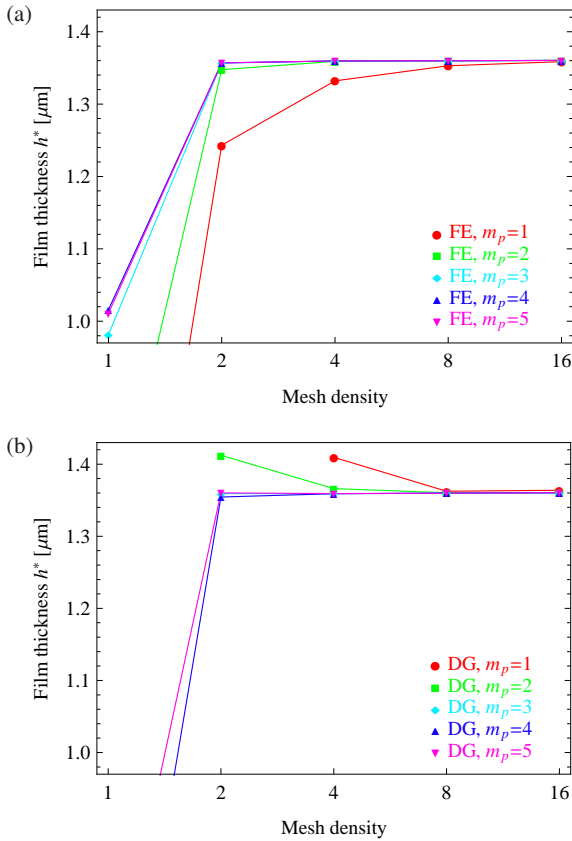


Fig. 16 Convergence of parameter $h^* = q/\bar{u}$ with mesh refinement for (a) FE and (b) DG treatment of the Reynolds equation (outstroke, $p_s = 1$ MPa, $U = 400$ mm/s).

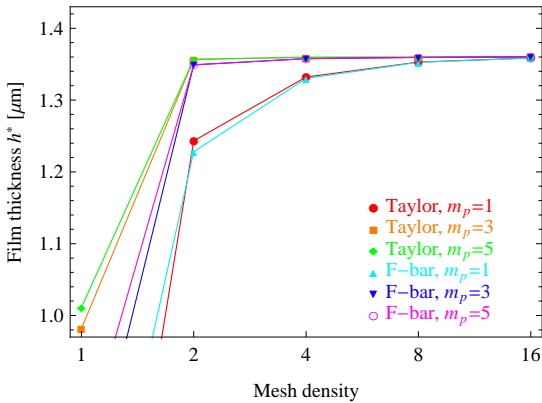


Fig. 17 O-ring seal: effect of solid element formulation on the convergence of parameter $h^* = q/\bar{u}$ with mesh refinement (FE treatment of the Reynolds equation).

in Fig. 19 for the sealed pressure $p_s = 5$ MPa, i.e. the highest pressure considered in the O-ring example. In the case of outstroke, the film thickness is approximately 7% smaller if the pressure dependence of viscosity is neglected, while in the case of instroke the difference is below 1%. In all cases, the pressure profiles are not visibly affected so the corresponding diagrams are not provided here.

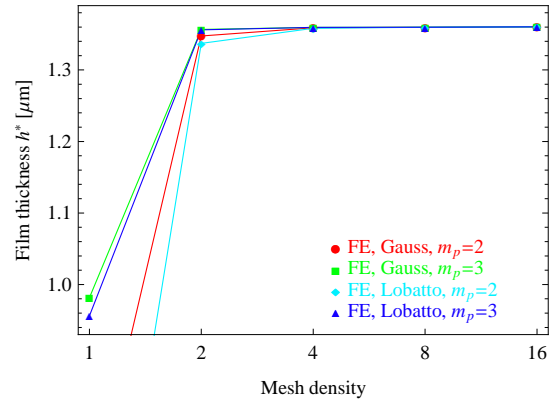


Fig. 18 O-ring seal: effect of quadrature (Gauss or Lobatto) on the convergence of parameter $h^* = q/\bar{u}$ with mesh refinement.

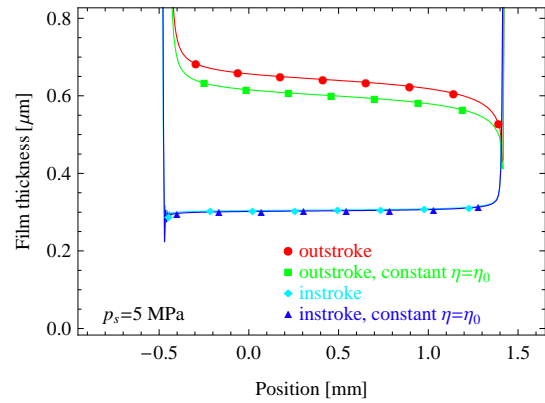


Fig. 19 Effect of pressure dependence of viscosity on the film thickness h (sealed pressure $p_s = 5$ MPa, rod speed $U = 100$ mm/s).

In the case of outstroke, the inlet zone, which governs lubricant entrainment, is at the sealed-pressure side. Thus, if the piezo-viscous effect is accounted for, the viscosity increases with increasing sealed pressure and, as a result, the film thickness increases. At instroke, the inlet zone is at the air side and the viscosity is essentially constant. Hence the difference between the outstroke and instroke as regards the influence of the piezo-viscous effect.

The effect of pressure dependence of viscosity on the leakage rate is illustrated in Fig. 20. Consistently with the results shown in Fig. 19, the leakage rate is only visibly affected in the case of outstroke and, as could be expected, the difference increases with increasing sealed pressure.

6 Conclusions

A computational scheme has been developed for the analysis of soft EHL problems in the finite deformation regime with application for reciprocating elastomeric seals. The seal is modelled as a hyperelastic body, and the flow of the lubricant is governed by the Reynolds equation. The finite element formulation is derived from the respective variational

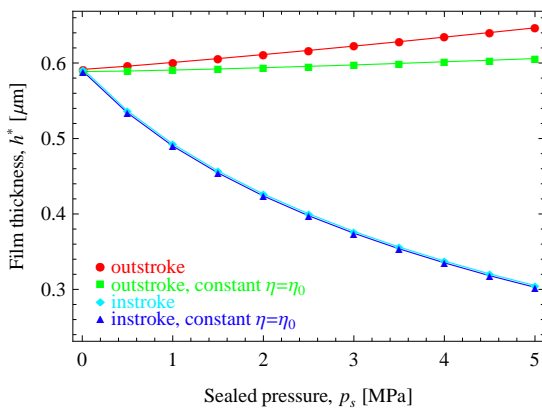


Fig. 20 Effect of pressure dependence of viscosity on the leakage rate represented by parameter $h^* = q/\bar{u}$ (rod speed $U = 100$ mm/s).

weak forms and the resulting nonlinear equations are solved monolithically for all global unknowns using the iterative Newton method.

Performance of the proposed numerical scheme has been assessed by studying the effect of mesh density and pressure interpolation order. It has been observed that spurious oscillations of the solution may occur in severe lubrication conditions, for instance, at low rod speeds. Looking for a remedy, a discontinuous Galerkin treatment of the Reynolds equation has been introduced as an alternative to the more usual continuous finite element method. However, the obtained results indicate that, in terms of accuracy and stability, the discontinuous Galerkin method actually performs worse, although the effect is not much pronounced.

The spurious oscillations are eliminated, or reduced, when the finite element mesh is refined. Also, it has been observed that the more severe the lubrication conditions the finer mesh is necessary to guarantee an oscillation-free solution. For a fixed mesh density, the accuracy of the solution can be improved by increasing the pressure interpolation order m_p , however, oscillations are not much affected by the pressure interpolation order. It seems that $m_p = 4$ is a reasonable choice. Mild oscillations, appearing in the vicinity of the dip in film thickness, do not significantly affect the predictions of the overall dynamic sealing performance.

In this work, a structured finite element mesh has been used with uniform mesh size along the lubricated boundary so that the same mesh could be used for the whole range of process parameters (note that the size of the actual contact zone depends on the sealed pressure, and much more weakly on the rod speed). Application of more optimal unstructured meshes, possibly refined adaptively, might result in substantial improvement of numerical efficiency and accuracy.

Finally let us note that the effect of surface roughness is not included in the present model. An idealized EHL problem for smooth surfaces is thus considered and an assumption of full-film hydrodynamic lubrication is implicitly adopted. Considering that the predicted film thickness is in some cases well below $1 \mu\text{m}$, the related effects can be significant if the

influence of surface roughness is accounted for, for instance, using the flow-factor approach, cf. [3; 9; 21; 25].

Acknowledgements This work has been partially supported by the European Commission through the PROHIPP project (NMP 2-CT-2004-505466).

References

- Adams M, Briscoe B, Johnson S (2007) Friction and lubrication of human skin. *Tribol Lett* 26:239–253
- Alart P, Curnier A (1991) A mixed formulation for frictional contact problems prone to Newton like solution methods. *Comp Meth Appl Mech Eng* 92:353–375
- Almqvist A, Dasht J (2006) The homogenization process of the Reynolds equation describing compressible liquid flow. *Tribol Int* 39:994–1002
- Baumann C, Oden J (1999) A discontinuous hp finite element method for convection-diffusion problems. *Comp Meth Appl Mech Eng* 175:311–341
- Dowson D (1995) Elastohydrodynamic and micro-elastohydrodynamic lubrication. *Wear* 190:125–138
- Dowson D, Higginson G (1977) *Elasto-hydrodynamic Lubrication*. Pergamon Press
- Hamrock B, Schmid S, Jacobsen B (2004) *Fundamentals of Fluid Film Lubrication*, 2nd edn. Marcel Dekker, New York
- Hughes C, Elcoate T, Evans H (1999) A novel method for integrating first and second order differential equations in elastohydrodynamic lubrication for the solution of smooth isothermal, line contact problems. *Int J Num Meth Eng* 44:1099–1113
- Jai M, Bou-Said B (2002) A comparison of homogenization and averaging techniques for the treatment of roughness in slip-flow-modified Reynolds equation. *Trans ASME J Tribol* 124:327–335
- Jones M, Fulford G, Please C, McElwain D, Collins M (2008) Elastohydrodynamics of the eyelid wiper. *Bull Math Biol* 70:323–343
- Korelc J (2002) Multi-language and multi-environment generation of nonlinear finite element codes. *Engineering with Computers* 18:312–327
- Korelc J (2006) *AceGen and AceFEM user manuals*. Available at <http://www.fgg.uni-lj.si/Symech/>
- Korelc J, Wriggers P (1997) Improved enhanced strain four-node element with Taylor expansion of the shape functions. *Int J Num Meth Eng* 40:407–421
- Lu H, Berzins M, Goodyer C, Jimack P (2005) High-order discontinuous Galerkin method for elastohydrodynamic lubrication line contact problems. *Commun Num Meth Eng* 21:643–650
- Lu H, Berzins M, Goodyer C, Jimack P, Walkley M (2006) Adaptive high-order finite element solution of transient elastohydrodynamic lubrication problems. *Proc Instn Mech Engrs Part J: J Engng Tribol* 220:215–225
- Müller H, Nau B (1998) *Fluid Sealing Technology, Principles and Applications*. Marcel Dekker, Inc.
- Nau B (1999) An historical review of studies of polymeric seals in reciprocating hydraulic systems. *Proc Instn Mech Engrs Part J: J Engng Tribol* 213:215–226
- Nikas G (2003) Elastohydrodynamics and mechanics of rectangular elastomeric seals for reciprocating piston rods. *Trans ASME J Tribol* 125:60–69
- Nikas G, Sayles R (2004) Nonlinear elasticity of rectangular elastomeric seals and its effect on elastohydrodynamic numerical analysis. *Tribol Int* 37:651–660
- Oh K, Rohde S (1977) Numerical solution of the point contact problem using the finite element method. *Int J Num Meth Eng* 11:1507–1518

21. Patir N, Cheng H (1978) An average flow model for determining effects of three-dimensional roughness on partial hydrodynamic lubrication. *Trans ASME J Lubr Technol* 100:12–17
22. Pietrzak G, Curnier A (1999) Large deformation frictional contact mechanics: continuum formulation and augmented Lagrangian treatment. *Comp Meth Appl Mech Engng* 177(3–4):351–381
23. Prati E, Strozzi A (1984) A study of the elastohydrodynamic problem in rectangular elastomeric seals. *Trans ASME J Tribol* 106:505–512
24. Ruskell L (1980) A rapidly converging theoretical solution of the elastohydrodynamic problem for rectangular rubber seals. *Proc Instn Mech Engrs Part C: J Mech Engng Sci* 22:9–16
25. Salant R, Maser N, Yang B (2007) Numerical model of a reciprocating hydraulic rod seal. *Trans ASME J Tribol* 129:91–97
26. Schellekens J, de Borst R (1993) On the numerical integration of interface elements. *Int J Num Meth Engng* 36:43–66
27. de Souza Neto E, Perić D, Dutko M, Owen D (1996) Design of simple low order finite elements for large strain analysis of nearly incompressible solids. *Int J Sol Struct* 33:3277–3296
28. Stupkiewicz S, Marcinişzyn A (2009) Elastohydrodynamic lubrication and finite configuration changes in reciprocating elastomeric seals. *Tribol Int* 42:615–627
29. de Vicente J, Stokes J, Spikes H (2005) The frictional properties of Newtonian fluids in rolling–sliding soft-EHL contact. *Tribol Lett* 20:273–286
30. Wriggers P (2002) *Computational Contact Mechanics*. Wiley, Chichester
31. Wu S (1986) A penalty formulation and numerical approximation of the reynolds-hertz problem of elastohydrodynamic lubrication. *Int J Engng Sci* 24:1001–1013
32. Yang Y, Hughes W (1983) An elastohydrodynamic analysis of preloaded sliding seals. *ASLE Trans* 27:197–202
33. Zienkiewicz O, Taylor R (2000) *The Finite Element Method*, 5th edn. Butterworth-Heinemann, Oxford
34. Zienkiewicz O, Taylor R, Sherwin S, Peiro J (2003) On discontinuous Galerkin methods. *Int J Num Meth Engng* 58:1119–1148